

See discussions, stats, and author profiles for this publication at: <https://www.researchgate.net/publication/263746244>

Preparation, Applications, and Digital Simulation of Carbon Interdigitated Array Electrodes

ARTICLE *in* ANALYTICAL CHEMISTRY · JULY 2014

Impact Factor: 5.64 · DOI: 10.1021/ac5019364 · Source: PubMed

CITATIONS

3

READS

22

3 AUTHORS, INCLUDING:



Bruce A Parkinson

University of Wyoming

251 PUBLICATIONS 7,037 CITATIONS

[SEE PROFILE](#)

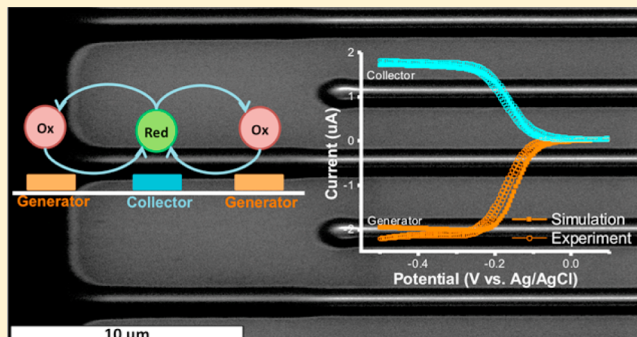
Preparation, Applications, and Digital Simulation of Carbon Interdigitated Array Electrodes

Fei Liu, Grigory Kolesov, and B. A. Parkinson*

Department of Chemistry and Department of Physics, School of Energy Resources, University of Wyoming, Laramie Wyoming 82071, United States

 Supporting Information

ABSTRACT: Carbon interdigitated array (IDA) electrodes with features sizes down to $1.2\text{ }\mu\text{m}$ were fabricated by controlled pyrolysis of patterned photoresist. Cyclic voltammetry of reversible redox species produced the expected steady-state currents. The collection efficiency depends on the IDA electrode spacing, which ranged from around 2.7 to $16.5\text{ }\mu\text{m}$, with the smaller dimensions achieving higher collection efficiencies of up to 98%. The signal amplification because of redox cycling makes it possible to detect species at relatively low concentrations (10^{-5} molar) and the small spacing allows detection of transient electrogenerated species with much shorter lifetimes (submillisecond). Digital simulation software that accounts for both the width and height of electrode elements as well as the electrode spacing was developed to model the IDA electrode response. The simulations are in quantitative agreement with experimental data for both a simple fast one electron redox reaction and an electron transfer with a following chemical reaction at the IDAs with larger gaps whereas currents measured for the smallest IDA electrodes, that were larger than the simulated currents, are attributed to convection from induced charge electrokinetic flow.



Microscale interdigitated array (IDA) electrodes, when compared to more macroscale electrodes, have attracted significant attention because of their sensitivity, high signal-to-noise ratio, and relatively low capacitive charging currents. Because of these favorable characteristics, IDA electrodes have been applied to fields like biochemical sensing, trace electroanalysis and field-flow-fractionation separations.^{1–4} IDA electrodes are also applied in electrochemical reactions where electroactive products produced at one electrode can be detected at the other electrode, much like in rotating ring-disk (RRDE) voltammetry. Unstable electroactive intermediates with submillisecond lifetimes can be detected whereas in RRDE voltammetry lifetimes need to be 10 ms or more. Additionally IDA electrodes are less noisy and more compact than RRDEs making them cheaper and easier to use in small-scale experiments and in glove boxes.

The fabrication of IDA electrodes has benefited greatly from highly developed photolithography techniques. Patterns on the micron scale can be easily fabricated and various designs and sizes of platinum or gold IDA electrodes have been constructed.^{5–7} Although the fabrication of metal IDA electrodes is relatively easy their application in electrochemical studies can be limited by the small potential window partly due to the catalytic activity of the commonly used electrode materials such as platinum in protic solvents. Conductive carbon materials are less reactive in general and therefore exhibit smaller background currents and larger potential windows,⁸ motivating their use for the fabrication of IDA electrodes.^{9–11}

There are two main methods to fabricate carbon IDAs: (1) A carbon film is initially deposited on an electrically insulating

substrate followed by deposition of a protective positive photoresist that is patterned and developed using photolithography. Subsequent removal of the unprotected carbon with dry etching and dissolve of the remaining photoresist leaves a patterned carbon IDA on the substrate.¹⁰ (2) Photolithography or electron beam lithography is used to prepare a photoresist pattern on a nonconductive substrate and the resist is subsequently pyrolyzed in forming gas to reduce the photoresist polymer to carbon IDA patterns.¹² Various carbon structures have been made from these methods.^{9,11,13–17} Among these, electrochemical study of carbon band electrodes with band widths down to 140 nm have been reported.^{16–18} However, it is difficult to achieve this small size on an IDA pattern since IDA electrodes usually require a large number of closely placed precise and electrically isolated digits.

There are two significant challenges for the preparation of high-quality carbon IDA electrodes that have limited their commercial availability and use: (1) The adhesion of the carbon layer to the substrate can be weak, which has been pointed out in several papers,^{19–21} and (2) the poor conductivity of some carbon films results in a large *iR* drop that is particularly troublesome for carbon IDAs with small feature sizes.^{11,19–22} Two recent papers^{16,17} demonstrated carbon IDA electrodes with relatively small sizes showing enhanced redox amplification, however, as we

Received: March 1, 2014

Accepted: July 6, 2014

Published: July 6, 2014



mentioned above, the cyclic voltammograms showed a large iR drop making it difficult to produce quantitative measurements.

In this article, we describe the fabrication of microscale carbon IDA electrodes with various gap sizes by photoresist pyrolysis and address both adhesion and conductivity issues. A digital simulation code for modeling the current, voltage and time behavior of IDA electrodes was developed and results from experiments, digital simulation, and analytical expressions are quantitatively compared for simple electron transfer reactions and coupled electrochemical-chemical (EC) reactions.

EXPERIMENTAL SECTION

Chemicals and Apparatus. Hexaammine ruthenium(III) chloride (Strem Chemicals, Inc.), potassium chloride (EMD Chemicals, Inc.), *N,N*-Dimethyl-p-phenylenediamine (Sigma-Aldrich Co. LLC.), and sodium hydroxide (Sigma-Aldrich Co. LLC.) were used as purchased. Electrochemical experiments were performed with a dual potentiostat (Ivium Technologies, Netherlands). A MA6/BA6 Mask Aligner (SUSS MicroTec, Germany) was used for photolithography. A scanning electron microscope (FEI corporate Quanta FEG 450), Raman spectrometer (IM-52, Snowy Range Instruments), and atomic force microscope (Asylum Research Cypher Scanning Probe Microscope) were used for physical characterization.

Carbon IDA Fabrication. Carbon IDA electrodes were fabricated on insulating surface-oxidized silicon wafers at the Center for Nanoscale Materials at Argonne National Laboratory. A photoresist layer with a thickness of around 1.5 μm was spin-coated onto the substrate and a MA6 Mask Aligner was then used for UV light exposure. After development, the IDA photoresist patterns were pyrolyzed in a 5% H_2 95% N_2 atmosphere with temperature increasing at a rate of 2 $^{\circ}\text{C}/\text{min}$ to 1000 $^{\circ}\text{C}$ and kept at this temperature for 1 h to reduce the photoresist to carbon (Supporting Information Figure S1). The furnace was then cooled down to room temperature at a cooling rate of 2 $^{\circ}\text{C}/\text{min}$.²³ To overcome the adhesion problem, several different photoresists were tried (s1813, AZ5214E and SU8 2002) and the resulting electrodes were electrochemically tested in both aqueous solution and organic solution. The carbon IDA made from SU8 had the best adhesion to the substrate. SiC formed at the interface between the silicon substrate and carbon pattern apparently acts as an adhesion layer.¹⁸ Subsequently, the carbon contact bars on the outside of the IDA electrodes were covered with a Surlyn film leaving only the “finger” areas exposed to the electrolyte for the electrochemical experiments. The fabricated carbon IDA electrodes had 50 pairs of microband electrodes, with a length of 1000 μm and with various designed dimensions of electrode widths and gaps between the electrodes (\sim 2 to 3 μm widths and \sim 2–16 μm gaps). The actual width of the microband electrodes is usually smaller than the designed size due to shrinkage during photoresist developing and pyrolysis. All reported IDA sizes are actual width and gap sizes measured by SEM.

Digital Simulations. The digital simulations were carried out using the finite difference method on an exponential grid.⁵ Fick’s diffusion law and the reaction kinetics govern the concentration of the species in the solution. The drift currents can be neglected due to the presence of excess electrolyte species in the solution. Thus, for example for a simple reversible reaction between species A and B, the equation for the concentration of species A, can be written as follows:

$$\frac{\partial[\text{A}]}{\partial t} = D\nabla^2[\text{A}] - k_f^{\text{AB}}[\text{A}] + k_b^{\text{AB}}[\text{B}] \quad (1)$$

Here D is the diffusion coefficient (assumed to be homogeneous) and k_f^{AB} and k_b^{AB} are forward and backward reaction electron

transfer rates, respectively. Finite difference methods are used to solve these equations by representing space as a grid and time as finite increments. For instance, the previous equation discretized on a uniform space grid reads

$$\frac{[\text{A}](r_{ijk}, t + \Delta t)}{\Delta t} = -k_f^{\text{AB}}[\text{A}](r_{ijk}, t) + k_b^{\text{AB}}[\text{B}](r_{ijk}, t) + D \sum_{\hat{x}_n=\hat{x}, \hat{y}, \hat{z}} \frac{[\text{A}](r_{ijk} + \Delta x_n \hat{x}_n, t) - 2[\text{A}](r_{ijk}, t) + [\text{A}](r_{ijk} - \Delta x_n \hat{x}_n, t)}{\Delta x_n^2} \quad (2)$$

Where r_{ijk} describes position of grid cell indexed by (i, j, k) , $\hat{x}, \hat{y}, \hat{z}$ are Cartesian unit vectors, Δx_n is the grid spacing in dimension n and Δt is the finite time step.

For IDAs, particularly those with features below the 8 μm level, the situation is complicated by the fact that the diffusion in both x and y dimensions affects the outcome, whereas z runs along the length of the electrodes and is treated as if it were infinite (i.e., edge effects are neglected). Dividing a 2D space into equally sized cells requires enormous amounts of computer memory, therefore a standard exponentially expanding grid^{24–26} was applied, except in the region occupied by the electrodes where a uniform grid spacing was set up in the x direction. Initially the electrodes were assumed to be flat or coplanar with the substrate but when deviations from the simulations were noticed at small electrode spacings, the simulation was expanded to incorporate the height of the IDA fingers where the electrode shapes are approximated by the blocks on a uniform grid. To achieve this, the exponential/uniform grid was used, where the exponential grid was set up to expand from the uppermost, left- and right-most surfaces of the electrodes (see Figure 1). Thus, the grid in y -direction is described as

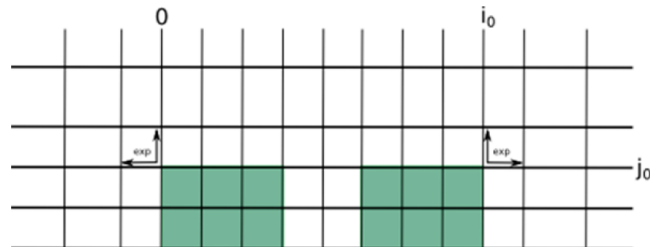


Figure 1. Exponential grid for digital simulations of IDAs with finite height electrodes. Darker blockers represent electrodes. Arrows mark the beginning of the exponential and end of the uniform grids. Actual grid dimensions are less than those depicted.

$$D_{2j}^* = \begin{cases} D^* e^{2\beta(\frac{3}{4}-j')}, & j' \geq 1 \\ D^* \frac{2(e^{\beta/2}+1)}{3+e^{\beta/2}}, & j' = 0 \\ D^* & j' < 0 \end{cases}$$

$$D_{1j}^* = \begin{cases} D^*(e^{\beta/2}+1) & j' = 0, \text{ at electrode} \\ 2D^* & j' < 0, \text{ at electrode} \end{cases}$$

$$D_{1j}^* = \begin{cases} D^* e^{2\beta(\frac{5}{4}-j')}, & j' \geq 2 \\ D^* \frac{2(e^{\beta/2}+1)}{3+e^{\beta/2}}, & j' = 1 \\ D^* & j' \leq 0 \end{cases}$$

$$D^* = D \frac{\Delta t}{\Delta y^2}$$

Here, D^* is the dimensionless diffusion coefficient, D_{jj}^* and D_{ijj}^* are up and down diffusion coefficients for a grid cell, $j, j' = j - j_0$, j_0 describes the start of the exponential grid and β is an expansion parameter of the grid typically set to 0.5.

Figure 1 shows the exponential/uniform grid used in the simulation to account for the finite height of the IDA electrodes. The grid size is changeable depends on how many blocks are used to present the electrode shape. Simulations with different block numbers gave very similar results (example is given in Supporting Information Figure S2). To save calculation time, less block number was preferred in our simulation. The exponential grid starts at $(0, j_0)$ and (i_0, j_0) cells. For details of calculation of diffusional fluxes on an exponential grid we refer the reader to ref 5.

We used the Butler–Volmer formulation for electron transfer reactions on the electrodes to calculate the forward and backward rate constants.

$$k_f = k^0 e^{-\alpha f(E-E^0)} \quad (3)$$

$$k_b = k^0 e^{-(1-\alpha)f(E-E^0)} \quad (4)$$

where k^0 is the standard rate constant, α is the transfer coefficient, and E^0 is the standard potential. In the simulations presented in this paper, the electron transfer reactions were assumed to be nernstian, that is, equilibrium concentrations of the species on the electrode surfaces were calculated at each time step. For chemical reactions in solution, the approach described in the ref 14 was applied;²⁴ that is, the reaction was explicitly discretized as in example above.

We used a periodic boundary condition (PBC) to speed up the calculations for the electrode arrays. In this approach the simulation was setup with only one pair of electrodes while the gap space after the second electrode was looped back onto the first electrode. After the simulation, the total current was calculated by multiplying by the number electrode pairs. We have checked the computation that utilized the PBC vs the full calculation that simulated all 100 electrodes in an IDA and found no significant differences in the simulated currents since only 2% of the electrodes are at a boundary.

RESULTS AND DISCUSSION

Physical Characterization and Working Principle of Carbon IDA Electrodes. Figure 2 shows optical and SEM images of a carbon IDA electrode, the latter showing the high fidelity and precision of the photolithographic and pyrolysis process. The Raman spectrum of a carbon IDA (Supporting Information Figure S3) shows two characteristic features, a broad peak at around 1357 cm^{-1} and a peak at 1606 cm^{-1} , that are assigned to a diamond-like peak and graphitic peak (G band) respectively,^{27,28} indicating a high sp^2 content and implying a structure close to glassy carbon. AFM imaging of a carbon IDA electrode was used to provide an accurate height of the fingers to be incorporated into the digital simulation (Supporting Information Figure S4). The height of the carbon IDA fingers is near 400 nm, much higher than most metal IDA electrodes.⁵

Like a rotating ring-disk electrode (RRDE), IDA electrodes have two working electrodes that are electrically isolated but instead of being concentric the electrodes are interdigitated with one set of “fingers” separate from another set of “fingers” with micron-sized gaps (Figure 3a). A bipotentiostat can independently control the potentials applied to the two working electrodes. Identified by function, one set of electrodes is called the generator and the other set is called the collector, analogous

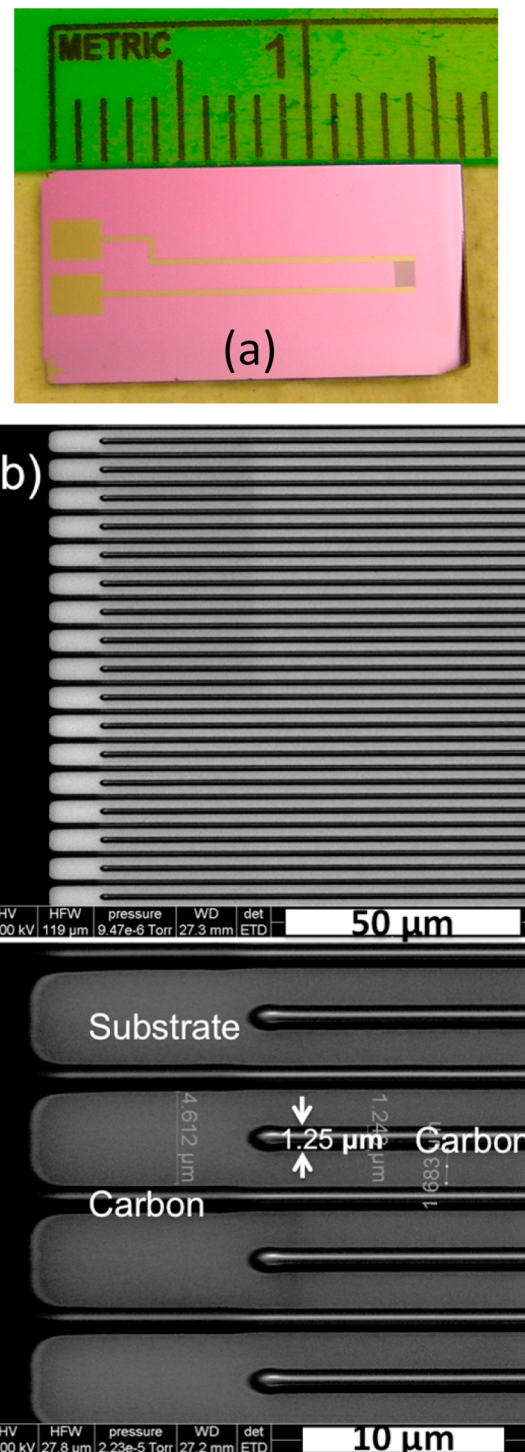


Figure 2. (a) Photograph of one of our carbon IDA electrodes. (b) SEM images of a carbon IDA electrode (1.25 μm width and 1.7 μm gap) showing many interdigitated fingers (above) and a higher magnification image of portions of four sets of fingers (below).

to the disk and the ring in a RRDE. For instance, an electroactive compound could be reduced on the generator and the product can diffuse to an adjacent collector electrode, set at a more positive potential, and get reoxidized to its initial state. Unlike the RRDE, the products from the collector can diffuse back to a generator electrode resulting in cycling or feedback that amplifies the current on both the generator and the collector electrodes (Figure 3b). Since mass transport is diffusive rather than

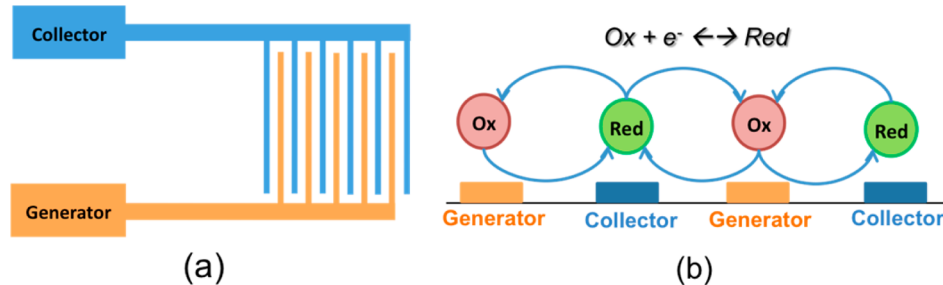


Figure 3. (a) Schematic view of IDA structure. (b) Generation/collection/regeneration process of an interdigitated array (IDA) electrode.

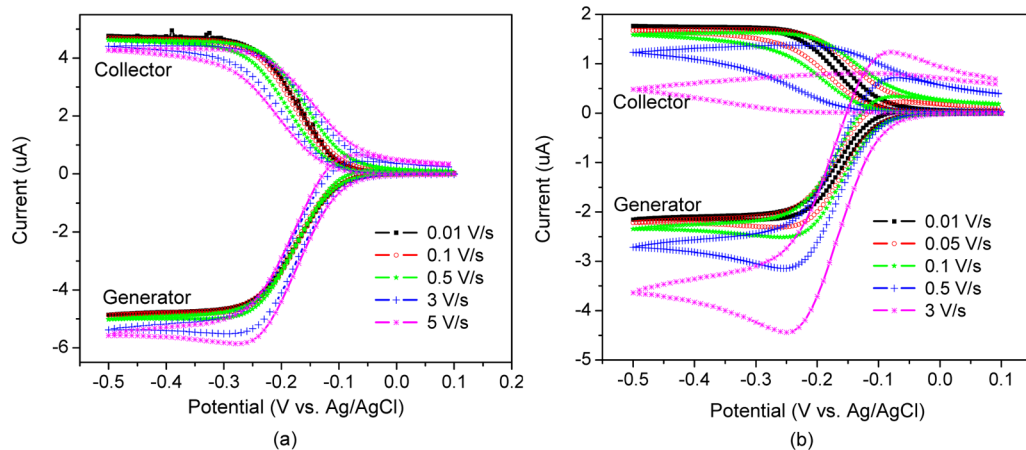


Figure 4. Cyclic voltammetry of 1 mM $\text{Ru}(\text{NH}_3)_6^{3+}$ with 0.1 M KCl in aqueous solution. The generator carbon IDA electrode is scanned from 0.1 to -0.5 V , while the potential of the collector is held at 0.1 V : reference electrode, Ag/AgCl ; counter electrode, carbon rod; (a) $1.3\text{ }\mu\text{m}$ width and $2.7\text{ }\mu\text{m}$ gap carbon IDA and (b) $1.5\text{ }\mu\text{m}$ width and $16.5\text{ }\mu\text{m}$ gap IDA.

hydrodynamic as in a RRDE, IDA electrodes more closely parallel conditions at a static electrode in a quiescent solution.

Electrochemical Performance of the Carbon IDA Electrodes. Figure 4a shows a typical cyclic voltammogram for a carbon IDA with $1.3\text{ }\mu\text{m}$ finger widths for both generator and collector electrodes with a gap of $2.7\text{ }\mu\text{m}$. In general, IDA electrodes with smaller gaps have higher collection efficiencies (the ratio of collector current to generator current). A carbon IDA with a gap of $2.7\text{ }\mu\text{m}$ results in the current on the collector being roughly a mirror image of the generator current at a scan rate of 0.01 V/s (Figure 4a). The collection efficiency approaches 98% in this case, meaning almost all the product from the generator are reaching the collector. This compares to collection efficiencies in RRDEs of at best 35–40%.²⁹ When scanning the potential an electrode with a $2.7\text{ }\mu\text{m}$ gap showed a small scan rate dependence of the generator current (Figure 4a), whereas the $16.5\text{ }\mu\text{m}$ gap IDA showed a large increase in generator current and a decrease in collector current as the scan rate was increased (Figure 4b). A simple diffusion length calculation shows that a compound with a diffusion coefficient of $1 \times 10^{-5}\text{ cm}^2/\text{s}$ will take about 3.6 ms to diffuse across a $2.7\text{ }\mu\text{m}$ gap and 136 ms to diffuse across a $16.5\text{ }\mu\text{m}$ gap. A scan rate of 3 V/s takes only 400 ms to scan 1.2 V explaining the lack of feedback from a steady-state microband diffusion profile and the presence of diffusional peaks typical of a single isolated working electrode on the cyclic voltammogram for the $16.5\text{ }\mu\text{m}$ gap IDA (Figure 4b). Redox species cycle between the generator and collector electrodes whereas some diffuse away into the bulk solution. This redox cycling current amplification factor for reversible systems is inversely proportional to the electrode gap and greatly enhances the current on IDA electrodes up to 13 times on our smallest gap

IDA electrodes allowing detection of small concentrations of redox species (Supporting Information Figure S5).

Digital Simulation of the Electrochemical Response of Carbon IDA Electrodes. Digital simulation was used to quantitatively analyze the current response of the IDA electrodes. Earlier digital simulations⁵ of IDA electrodes ignored the height of the IDA “fingers” by using a flat or coplanar electrode model for the metal IDA electrodes. Our simulations results employing a coplanar electrode model showed good agreement between the simulation and experiment for the large gap IDA electrodes (16 and $8\text{ }\mu\text{m}$) but did not properly fit the voltammetric response of the small gap electrodes. AFM height measurements (Supporting Information Figure S4) reveals that the 400 nm height of the microband electrodes cannot be ignored in the digital simulations of small gap IDAs. Figure 5 shows an obvious difference between a digital simulation using a coplanar electrode model and a noncoplanar electrode model. The sides of microband electrodes may produce an enhanced feedback in the thin layer gaps between each microband electrode pair (Figure 6), accounting for the experimental currents being larger than the simulated currents using the coplanar electrode model for the $2\text{ }\mu\text{m}$ gap IDA electrodes.

Figure 7 compares the digital simulation using the noncoplanar model and the experimental results for a $16.5\text{ }\mu\text{m}$ gap IDA electrode at various scan rates. It shows good agreement between the simulation and experiment for the different scan rates. The deviation for the generator electrode at the faster scan rates (Figure 7c) is a result of the resistance of the microband electrodes coming in at the higher current levels.

The simulation of simple fast electron transfer reactions in aqueous solution for the various IDA sizes is compared with the

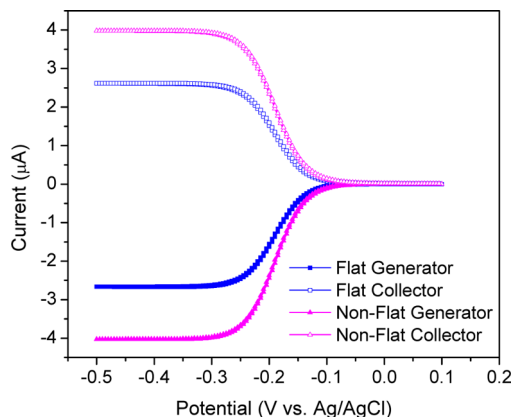


Figure 5. Comparison of digital simulation with flat electrode model and nonflat electrode model of IDA with 2 μm width electrodes and 2 μm gap.

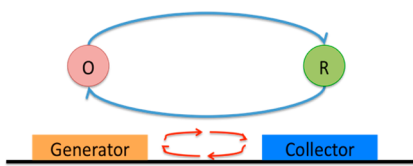


Figure 6. Drawing approximately to scale for a 2 μm electrode 2 μm gap IDA showing enhanced feedback (red arrows) and electrode area between each electrode pair.

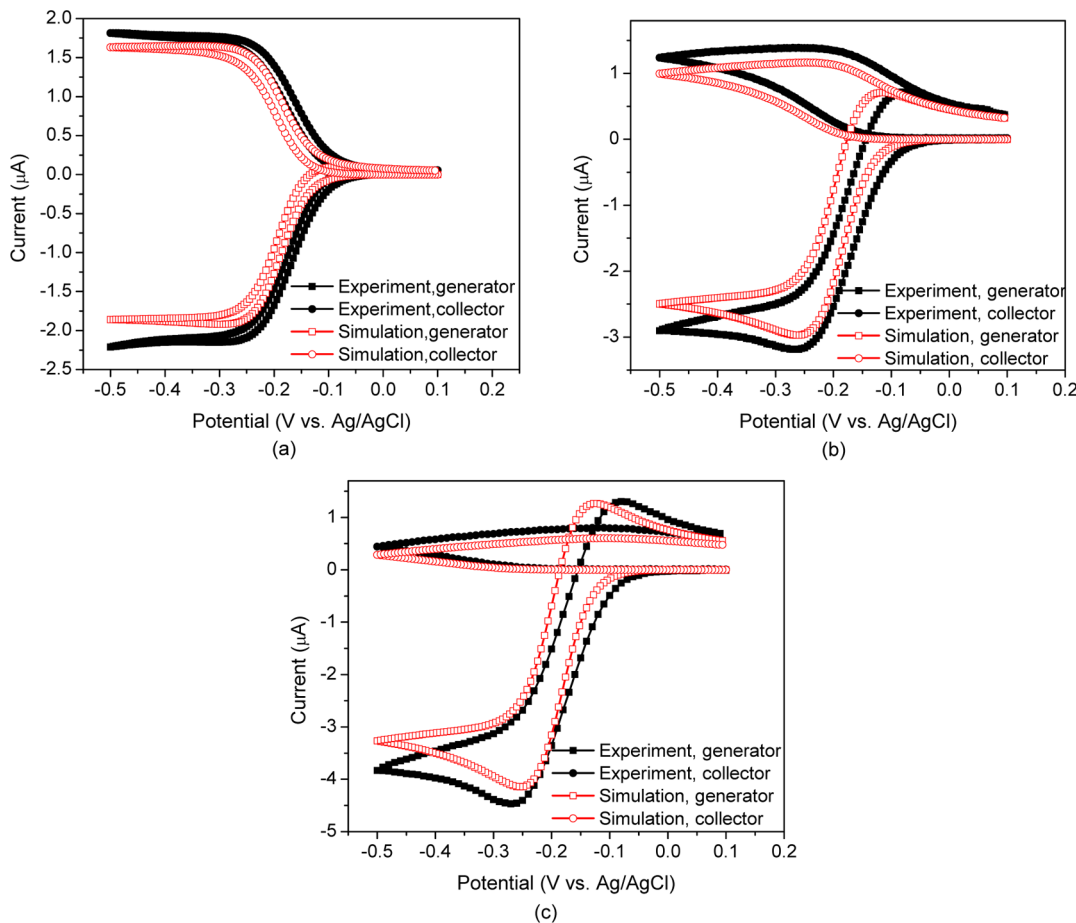


Figure 7. Comparison of experimental cyclic voltammetric curves with simulated curves under various scan rates for an IDA with a 16.5 μm gap and a width of 1.5 μm . One mM $\text{Ru}(\text{NH}_3)_6\text{Cl}_3$ with 0.1 M KCl aqueous solution: working electrode, carbon IDA with 16.5 μm gap; reference electrode, Ag/AgCl; counter electrode, carbon rod; (a) 0.01, (b) 0.5, and (c) 3 V/s.

experimental results in Figure 8. The simulations compare well with the experimental results except for some deviation for the IDA electrode with 2.7 μm gap. Collection efficiencies of different size carbon IDA with various scan rates was also measured in experiment and estimated with digital simulation, as shown in Supporting Information Figure S6.

This deviation between experiment and simulation is more significant when using a carbon IDA in the single working electrode mode where the collector is kept at open circuit. Cyclic voltammograms with the small gap IDAs at slow scan rates show the largest deviation for the oxidation of ferrocene in acetonitrile, (Figure 9a) whereas at higher scan rates the agreement with simulation improves (Figure 9b and c).

The deviation from the simulation at slow scan rates with small gap is perhaps due to an enhanced mass transfer leading to a larger measured current. This enhanced mass transfer may be a result from induced charge near a polarizable surface (like the silicon oxide substrate in this case), termed “induced charge electro-osmosis” (ICEO).³⁰ The effect of this well-known electrokinetic flow is quite apparent on slow scan cyclic voltammograms on the smallest gap IDA electrodes not operating in the generator collector mode as seen in Figure 9.

K Aoki et al.³¹ have calculated the steady-state limiting currents for IDA electrodes applicable to slower scan rates using an analytical expression (eq 5) where m is the number of microband electrodes, b is the length of the microband electrode,

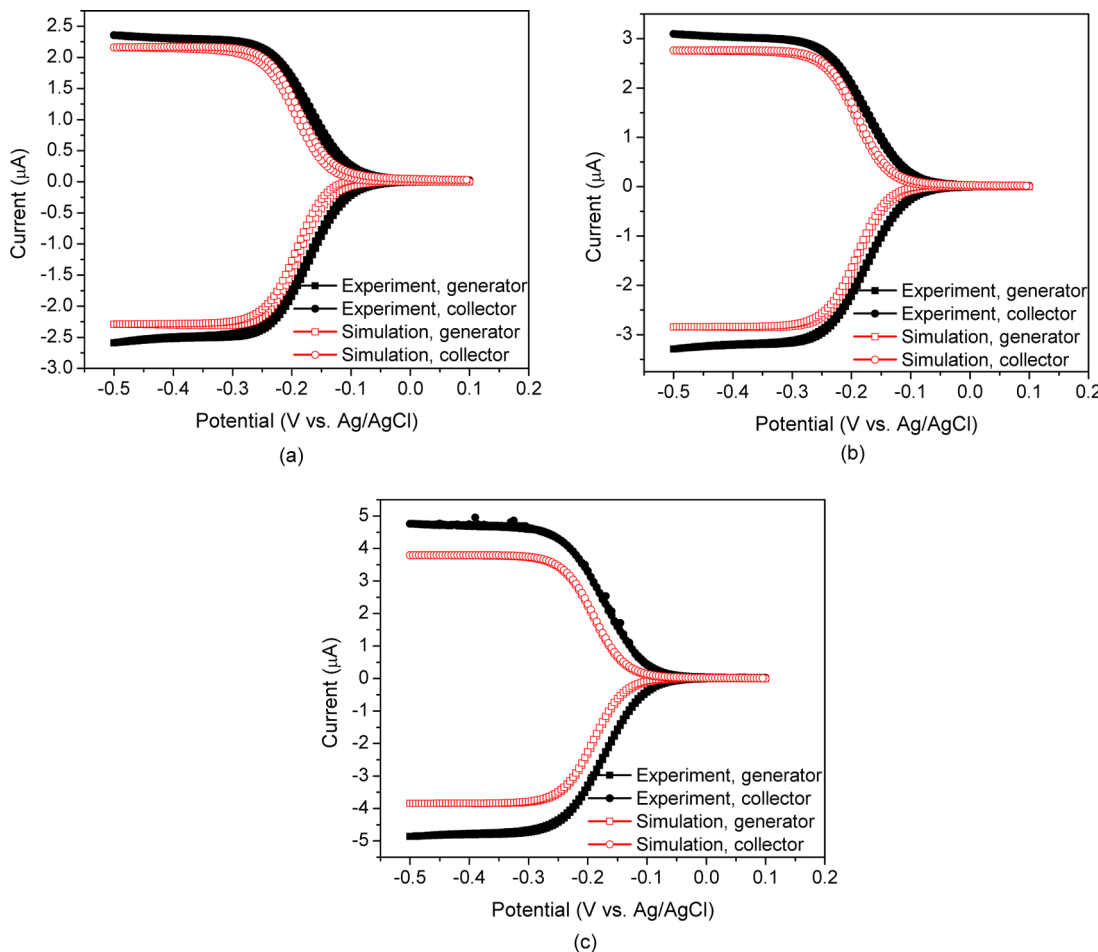


Figure 8. Comparison of experimental cyclic voltammetric curves with the simulated curves for carbon IDA electrodes of various dimensions. One mM $\text{Ru}(\text{NH}_3)_6\text{Cl}_3$ with 0.1 M KCl aqueous solution: working electrode, carbon IDA; reference electrode, Ag/AgCl; counter electrode, carbon rod; scan rate, 0.01 V/s; (a) 2.3 μm width, 8.7 μm gap; (b) 2.3 μm width, 4.7 μm gap; (c) 1.3 μm width, 2.7 μm gap.

n is the number of electrons, F is the Faraday constant, c^* is the bulk concentration, D is the diffusion coefficient, w_a is the width of the microband electrode, and w_g is the gap between adjacent microband electrodes.

$$|I_{\text{lim}}| = mbnFc^*D \left[0.637 \ln \left\{ 2.55 \left(1 + \frac{w_a}{w_g} \right) \right\} - \frac{0.19}{\left(1 + \frac{w_a}{w_g} \right)^2} \right] \quad (5)$$

A comparison between our experimental limiting currents, simulated limiting currents and the analytical calculation all agree quite well for the 16.5 and 16.7 μm gap IDAs but again deviate for smaller gap IDAs as shown in Figure 10. The measured current for the smaller gap IDA (2.7 μm) is much larger than predicted either with the digital simulation or eq 5 above. The larger current measured for the 2.7 μm gap IDA could also be from ICEO flow, that we speculated was responsible for the factor of 2 higher experimental current in the single electrode experiments, that is less of a factor in the larger total currents from redox cycling in the generator/collector mode.

IDA Electrodes and Digital Simulation For an EC Reaction. We now compare experimental results and simulations for a more complicated EC reaction (an electron transfer followed by a chemical reaction) at our carbon IDA electrodes.

We selected a well-studied EC reaction sequence with a relatively fast chemical step, the reversible two-electron oxidation/deprotonation of *N,N*-dimethyl-*p*-phenylenediamine, that is followed by the irreversible displacement of $\text{NH}(\text{CH}_3)_2$ (reaction 2).³² Cyclic voltammetry shows a decreased reduction current on the return scan at slow scan rates depending on the rate of the chemical step, k_c .

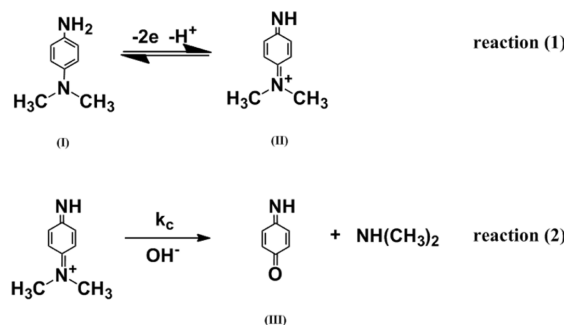


Figure 11 shows the comparison between the experimental and simulation results for the above reactions with a carbon IDA used as generator and collector electrodes. The potential of the collector was held at -0.15 V vs Ag/AgCl while the potential of the generator was swept between -0.2 and 0.3 V vs Ag/AgCl at a scan rate of 0.1 V/s. The simulation uses a model that includes the chemical step and a k_c of 40 s^{-1} and shows good agreement

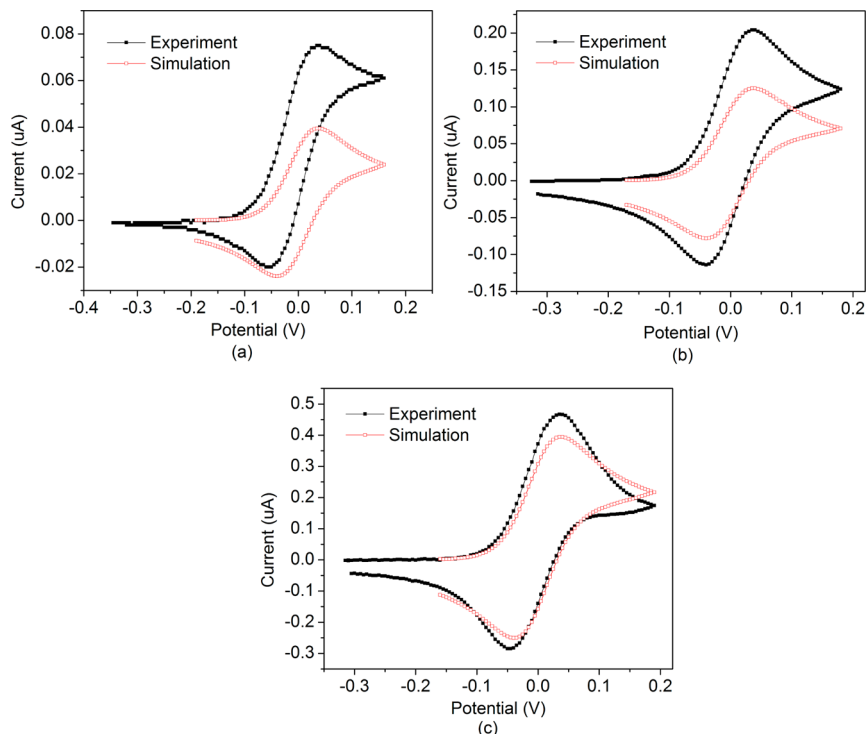


Figure 9. Comparison of single working electrode mode experimental cyclic voltammetric curves with simulated curves. 0.11 mM ferrocene in acetonitrile solution with 0.2 M tetrabutylammonium hexafluorophosphate as electrolyte: working electrode, carbon IDA with 2.7 μm width and 2.3 μm gap; reference electrode, Ag wire; counter electrode, carbon rod. Standard potential of ferrocene was adjust to 0 for all data: (a) 0.01, (b) 0.1, and (c) 1 V/s.

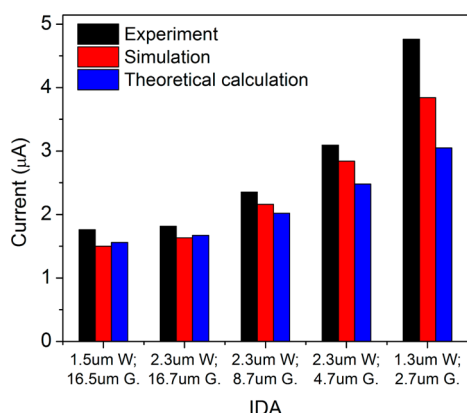


Figure 10. Comparison of the experimental results with calculated and simulated results for steady state currents in the generator/collector mode of various IDA geometries, "W" and "G" refer to the width and gap, respectively: solution, 1 mM $\text{Ru}(\text{NH}_3)_6\text{Cl}_3$ aqueous solution; working electrode, carbon IDA; RE, Ag/AgCl; counter electrode, carbon rod; scan rate, 10 mV/s.

with the experimental result where the collector current is much lower than the generator current as a result of the consumption of compound (II) from the following chemical reaction (reaction 2). The determined value of k_c from least-squares refinement is $\sim 40 \text{ s}^{-1}$ corresponding to a lifetime of 25 ms at pH 11.25, in good agreement with the value of 42 s^{-1} at pH 11.63 measured using a scanning electrochemical microscope.¹⁷

CONCLUSION

Carbon interdigitated array electrodes have been constructed using photolithography followed by the pyrolysis of the

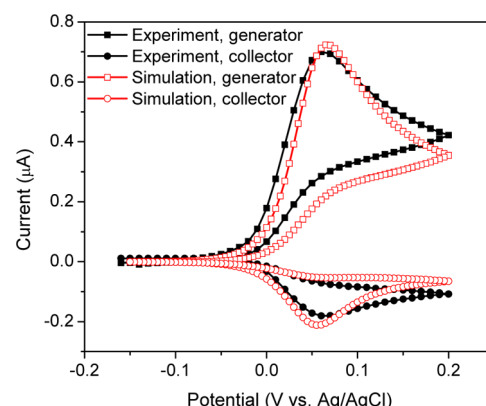


Figure 11. IDA electrode cyclic voltammetric results compared with the simulation for a simple EC reaction. Solution: 0.22 mM *N,N*-Dimethyl-p-phenyl-enediamine with 0.1 M KCl aqueous solution, pH = 11.25. WE: carbon IDA, 2.4 μm width and 4.6 μm gap. RE: Ag/AgCl. CE: carbon rod. Potential of the collector is held at -0.15 V vs Ag/AgCl. The scan rate is 0.1 V/s. The simulation uses the same reaction solution and working electrode conditions with a D of $5 \times 10^{-6} \text{ cm}^2/\text{s}$ and k_c of 40 s^{-1} .

photoresist to form carbon IDA structures with dimensions and gaps as small as 1.3 μm and have demonstrated exceptional electrochemical performance. Steady-state currents in the generator/collector mode were observed at slow scan rates with collection efficiencies as high as 98% on the IDAs with the smallest widths and gaps. A new digital simulation was developed that incorporates the three-dimensionality or noncoplanar nature of the electrode structures. The incorporation of the three dimensionality of the IDA electrodes into the in the generator/collector mode was particularly important for the small electrode gaps since enhanced of the redox cycling

reactions occur the gaps between adjacent IDA fingers that significantly enhances the currents. Good agreement between experimental measurements and the simulation was demonstrated for IDAs with larger gap sizes at faster scan rates, however some significant differences appeared for the smallest gap IDA electrodes at slow scan rates in the single working electrode mode. This deviation was proposed to result from “induced charge electro-osmotic flow” (ICEO) near a charged surface (the carbon IDA SiO₂ substrate) producing additional mass transfer near the electrode surface. The simulation for noncoplanar IDA electrodes in the generator/collector mode was applied to both simple fast electron transfer reactions and an electrochemical reaction followed by a chemical reaction (EC mechanism) where it produced a rate constant in agreement with literature values. The scalable fabrication of stable micron sized carbon IDA electrodes to apply to more complex electrochemical reactions, such as the classic four electron/four proton oxygen reduction reaction, and using digital simulation to investigate and verify mechanisms is now possible.

■ ASSOCIATED CONTENT

Supporting Information

Additional material as described in the text. This material is available free of charge via the Internet at <http://pubs.acs.org>.

■ AUTHOR INFORMATION

Corresponding Author

*E-mail: bparkin1@uwyo.edu.

Notes

The authors declare no competing financial interest.

■ ACKNOWLEDGMENTS

This work was supported as part of the Center for Molecular Electrocatalysis, an Energy Frontier Research Center funded by the Department of Energy, Office of Science Office of Basic Energy Science under FWP 56073. Use of the Center for Nanoscale Materials was supported by the U.S. Department of Energy, Office of Science, Office of Basic Energy Sciences, under Contract No. DE-AC02-06CH11357. Prof. Keith Carron and Prof. Brian Leonard are acknowledged for use of their Raman spectrometer and Dr. John Rowley for AFM measurements. We especially acknowledge Dr. Ralu Divan, Dr. Leo Ocola and Dr. Suzanne Miller in Center Nanoscale Materials, Argonne National Laboratory for their assistance in IDA fabrication.

■ REFERENCES

- (1) Varshney, M.; Li, Y. *Biosens. Bioelectron.* **2009**, *24*, 2951–2960.
- (2) Wang, X.-B.; Yang, J.; Huang, Y.; Vykoukal, J.; Becker, F. F.; Gascoyne, P. R. C. *Anal. Chem.* **2000**, *72*, 832–839.
- (3) Sheppard, N. F., Jr.; Tucker, R. C.; Wu, C. *Anal. Chem.* **1993**, *65*, 1199–1202.
- (4) Liu, D.; Perdue, R. K.; Sun, L.; Crooks, R. M. *Langmuir* **2004**, *20*, 5905–5910.
- (5) Bard, A. J.; Crayston, J. A.; Kittlesen, G. P.; Varco Shea, T.; Wrighton, M. S. *Anal. Chem.* **1986**, *58*, 2321–2331.
- (6) Niwa, O.; Xu, Y.; Halsall, H. B.; Heineman, W. R. *Anal. Chem.* **1993**, *65*, 1559–1563.
- (7) Ojima, H.; Umeda, M.; Mohamedi, M.; Uchida, I. *Electroanal* **2003**, *15*, 1677–1681.
- (8) McCreery, R. L. *Chem. Rev.* **2008**, *108*, 2646–2687.
- (9) Heo, J. I.; Shim, D. S.; Teixidor, G. T.; Oh, S.; Madou, M. J.; Shin, H. J. *Electrochim. Soc.* **2011**, *158*, J76.
- (10) Niwa, O.; Tabei, H. *Anal. Chem.* **1994**, *66*, 285–289.
- (11) Tabei, H.; Morita, M.; Niwa, O.; Horiuchi, T. *J. Electroanal. Chem.* **1992**, *334*, 25–33.
- (12) Kostecki, R.; Song, X. Y.; Kinoshita, K. *J. Electrochim. Soc.* **2000**, *147*, 1878–1881.
- (13) Wang, C.; Madou, M. *Biosens. Bioelectron.* **2005**, *20*, 2181–2187.
- (14) Kostecki, R.; Song, X.; Kinoshita, K. *Electrochim. Solid-State Lett.* **1999**, *2*, 465–467.
- (15) Kostecki, R.; Song, X.; Kinoshita, K. *Electrochim. Solid-State Lett.* **2002**, *5*, E29.
- (16) Kamath, R. R.; Madou, M. *J. Anal. Chem.* **2014**, *86*, 2963–2971.
- (17) Heo, J.-I.; Lim, Y.; Shin, H. *Analyst* **2013**, *138*, 6404.
- (18) Du, R.; Ssenyange, S.; Aktary, M.; McDermott, M. T. *Small* **2009**, NA–NA.
- (19) Huang, X.-J.; O’Mahony, A. M.; Compton, R. G. *Small* **2009**, *5*, 776–788.
- (20) Niwa, O.; Horiuchi, T.; Tabei, H. *J. Electroanal. Chem.* **1994**, *265*.
- (21) Morita, M.; Niwa, O.; Horiuchi, T. *Electrochim. Acta* **1997**, *42*, 3177–3183.
- (22) Fiacabrino, G. C.; Tang, X.-M.; Skinner, N.; De Rooij, N. F.; Koudelka-Hep, M. *Anal. Chim. Acta* **1996**, *326*, 155–161.
- (23) Ranganathan, S.; McCreery, R.; Majji, S. M.; Madou, M. J. *Electrochim. Soc.* **2000**, *147*, 277–282.
- (24) Shea, T. V.; Bard, A. J. *Anal. Chem.* **1987**, *59*, 2101–2111.
- (25) Feldberg, S. W. *J. Electroanal. Chem. Interfacial Electrochem.* **1981**, *127*, 1–10.
- (26) Arena, J. V.; Rusling, J. F. *Anal. Chem.* **1986**, *58*, 1481–1488.
- (27) Osswald, S.; Yushin, G.; Mochalin, V.; Kucheyev, S. O.; Gogotsi, Y. *J. Am. Chem. Soc.* **2006**, *128*, 11635–11642.
- (28) Tay, B. K.; Shi, X.; Tan, H. S.; Yang, H. S.; Sun, Z. *Surf. Coat. Technol.* **1998**, *105*, 155–158.
- (29) Albery, W. J.; Hitchman, M. L. *Ring-Disc Electrodes*; Clarendon Press, Oxford, 1971.
- (30) Bazant, M. Z.; Squires, T. M. *Curr. Opin. Colloid Interface Sci.* **2010**, *15*, 203–213.
- (31) Aoki, K.; Morita, M.; Niwa, O.; Tabei, H. *J. Electroanal. Chem. Interfacial Electrochem.* **1988**, *256*, 269–282.
- (32) Bard, A. J.; Denuault, G.; Friesner, R. A.; Dornblaser, B. C.; Tuckerman, L. S. *Anal. Chem.* **1991**, *63*, 1282–1288.